REPORT DOCUMENTATION PAGE

Form Approved
OMB No. 0704-0188

1. REPORT DATE *(DD-MM-YYYY)*	**2. REPORT TYPE**	**3. DATES COVERED** *(From - To)*
18-04-2005	Conference Paper POSTPRINT	2003 - 2005

4. TITLE AND SUBTITLE
An Integrated Systematic Approach to Linerless Composite Tank Development

5a. CONTRACT NUMBER
FA9453-03-C-0211
FA9453-03-C-0213

5b. GRANT NUMBER

5c. PROGRAM ELEMENT NUMBER
65502C

6. AUTHOR(S)
Kaushik Mallick, John Cronin, Kevin Ryan, Steven Arzberger, Naseem Munshi,
Chris Paul*, Jeffry S. Welsh*

5d. PROJECT NUMBER
1601

5e. TASK NUMBER
MV

5f. WORK UNIT NUMBER
DV/DX

7. PERFORMING ORGANIZATION NAME(S) AND ADDRESS(ES) AND ADDRESS(ES)
Composite Technology Development, Inc
2600 Campus Drive, Suite D
Lafayette, CO 80026

8. PERFORMING ORGANIZATION REPORT NUMBER

9. SPONSORING / MONITORING AGENCY NAME(S) AND ADDRESS(ES)
*Air Force Research Laboratory
Space Vehicles
3550 Aberdeen Ave SE
Kirtland AFB, NM 87117-5776

10. SPONSOR/MONITOR'S ACRONYM(S)
AFRL/VSSV

11. SPONSOR/MONITOR'S REPORT NUMBER(S)
AFRL-VS-PS-TP-2006-1046

12. DISTRIBUTION / AVAILABILITY STATEMENT
Approved for public release; distribution is unlimited. (Clearance #VS05-0267)

13. SUPPLEMENTARY NOTES
Published in the proceedings of the 46th AIAA/ASME/ASCE/AHS/ASC Structures, Structural Dynamics, and Materials Conference, 18 – 21 Apr 05, Austin, TX

14. ABSTRACT

The paper describes a program currently underway at Composite Technology Development, Inc. to dramatically improve the design and capabilities of lightweight linerless composite tanks. The program integrates material development and characterization, micromechanics-based analyses of composite materials and structural design and fabrication of prototype tanks. This integrated systematic approach, addresses the multi-scale and multi-disciplinary issues that are critical to linerless composite tank design by looking concurrently at material requirements, capabilities and tailoring, refinement of fabrication process, and structural design optimization. Unlike traditional composite over-wrapped pressure vessels, the linerless composite tanks depend on the composite shell itself to serve as a permeation barrier in addition to carrying all pressure and environmental loads. Designing these tanks requires accurate knowledge of the structural response of the tank on the macro-scale as well as the material behavior on the micro-scale. Limiting and managing the development of microcracks and microcrack-induced permeability in the composite shell dictates that new materials be tailored specially for this purpose. The paper describes how micromechanics-based analysis is used to: 1) define critical material-performance parameters that drive the development of new toughened matrices, and 2) predict microcrack formation and permeability in composite laminates under biaxial load. Key concepts are presented that help optimize the structural design of linerless composite tanks. Finally, the paper presents the progress to date in designing and fabricating linerless composite tanks using a newly developed, microcrack-resistant resin system.

15. SUBJECT TERMS
Space Vehicles, Composite Tanks; Linerless; ; Composite Shell; Composite Laminates; Permeability; Microcrack; Resin

16. SECURITY CLASSIFICATION OF:			**17. LIMITATION OF ABSTRACT**	**18. NUMBER OF PAGES**	**19a. NAME OF RESPONSIBLE PERSON**
a. REPORT	**b. ABSTRACT**	**c. THIS PAGE**	Unlimited	18	Jeffry Welsh
Unclassified	Unclassified	Unclassified			**19b. TELEPHONE NUMBER** *(include area code)* 505-846-7344

46th AIAA/ASME/ASCE/AHS/ASC Structures, Structural Dynamics & Materials Conference
18 - 21 April 2005, Austin, Texas

AIAA 2005-2089

An Integrated Systematic Approach to Linerless Composite Tank Development

Kaushik Mallick[*], John Cronin[†], Kevin Ryan[‡], Steven Arzberger[§] and Naseem Munshi[**]
Composite Technology Development, Inc., Lafayette, Colorado, 80026

Chris Paul[††] and Jeffry S. Welsh[‡‡]
Air Force Research Laboratory (AFRL/VSSV)
3550 Aberdeen Ave SE, Kirtland AFB, NM 87117-5776

Abstract

The paper describes a program currently underway at Composite Technology Development, Inc. to dramatically improve the design and capabilities of lightweight linerless composite tanks. The program integrates material development and characterization, micromechanics-based analyses of composite materials and structural design and fabrication of prototype tanks. This *integrated systematic approach*, addresses the multi-scale and multi-disciplinary issues that are critical to linerless composite tank design by looking concurrently at material requirements, capabilities and tailoring, refinement of fabrication process, and structural design optimization. Unlike traditional composite over-wrapped pressure vessels, the linerless composite tanks depend on the composite shell itself to serve as a permeation barrier in addition to carrying all pressure and environmental loads. Designing these tanks requires accurate knowledge of the structural response of the tank on the macro-scale as well as the material behavior on the micro-scale. Limiting and managing the development of microcracks and microcrack-induced permeability in the composite shell dictates that new materials be tailored specially for this purpose. The paper describes how micromechanics-based analysis is used to: 1) define critical material-performance parameters that drive the development of new toughened matrices, and 2) predict microcrack formation and permeability in composite laminates under biaxial load. Key concepts are presented that help optimize the structural design of linerless composite tanks. Finally, the paper presents the progress to date in designing and fabricating linerless composite tanks using a newly developed, microcrack-resistant resin system.

Nomenclature

p	=	internal pressure
R	=	internal radius of the tank
t	=	thickness of the laminate
σ_θ	=	hoop stress in a pressure vessel
σ_a	=	axial stress in a pressure vessel
$\pm\theta$	=	helical ply angle
G_{mc}	=	critical microcrack fracture toughness
D^{90}	=	microcrack density in a hoop ply

[*] Senior Project Manager, Kaushik@CTD-materials.com, email: kaushik@ctd-materials.com, AIAA member
[†] Design Engineer
[‡] Test Engineer
[§] Senior Chemist
[**] President
[††] Lt., Space Vehicles Directorate
[‡‡] Program Manager, Space Vehicles Directorate

$D^{\pm\theta}$ = microcrack density in a helical ply
E_θ = elastic modulus of the tank laminate in the hoop direction
E_a = elastic modulus of the tank laminate in the axial direction
α_θ = coefficient of thermal expansion of the tank laminate in the hoop direction
α_a = coefficient of thermal expansion of the tank laminate in the axial direction
ΔT = stress free temperature – test temperature
ω = damage variable
Q = fluid flow rate
ΔP = pressure differential through the tank laminate
ξ = empirical constant in permeability testing
ρ = normalized microcrack spacing

I. Introduction

Many future aircraft, launch vehicle, and spacecraft systems such as the Airborne Laser (ABL) system (Figure 1) will require linerless composite tanks for chemical storage, transport and/or mixing. Current state-of-the practice for such tanks includes metal and composite-overwrapped metal structures. Linerless composite tanks are being considered for these applications because of their potential to increase mission capabilities and lower production costs. These tanks are projected to offer up to 25 percent weight reduction compared to current conventional metal lined tanks, allowing increased chemical storage volume and/or reduced total system mass. If properly designed, linerless composite tanks can also reduce the operational risks and maintenance costs over their lifetime due to their inherently simple construction.

Figure 1. Air Borne Laser aircraft

The composite outer layer on traditional composite-overwrapped pressure vessels with metallic or polymeric liners is typically designed to safeguard against structural failure by rupture, while the liner is designed to contain the fluids.[1] In essence, the structural design of the tank is decoupled from the fluid containment requirement of the design. By contrast, linerless composite tanks require the composite shell to serve as a permeation barrier in addition to carrying all pressure and environmental loads. Understanding the microcracking, damage propagation and the resulting permeation of fluids at the tank's operating conditions is a primary criterion for optimizing the design of these tank structures. In essence, the design of linerless composite tanks requires a *paradigm shift* whereby accurate knowledge of both the structural response of the tank on the macro-scale as well as the material behavior on the micro-scale are required.

Ultimately, success in developing these new tanks will hinge on success in developing new materials that are specially tailored to satisfy both the macro-scale and the micro-scale requirements. These materials must also address concerns over long-term structural integrity, leakage due to microcracking, and contamination of composite materials.[2] To meet these challenging requirements, Composite Technology Development, Inc (CTD) has developed *an integrated systematic approach* that involves concurrent development of tank specifications, engineering and micromechanics models, purpose-designed composite materials, and innovative design and fabrication techniques, and addresses the multi-scale and multi-disciplinary issues that are critical in linerless tank design (see Figure 2). This integrated systematic approach looks concurrently at the totality of critical issues, including material capabilities and tailoring, fabrication process optimization, and structural design optimization.

The paper presents results of work to date at CTD to develop new and novel materials for linerless composite tanks. The following sections address progress in three primary areas of work: 1. Material Development, 2. Micromechanics, and 3. Design and Engineering of linerless composite tanks. As will be evident in the course of the paper, the success of CTD's integrated systematic approach depends on establishing an intimate inter-relationship between these focus areas. Consistent use of this approach has enabled CTD to make substantial advancements to the technology of linerless composite tanks. This is in sharp contrast to the broader industry, where previous efforts

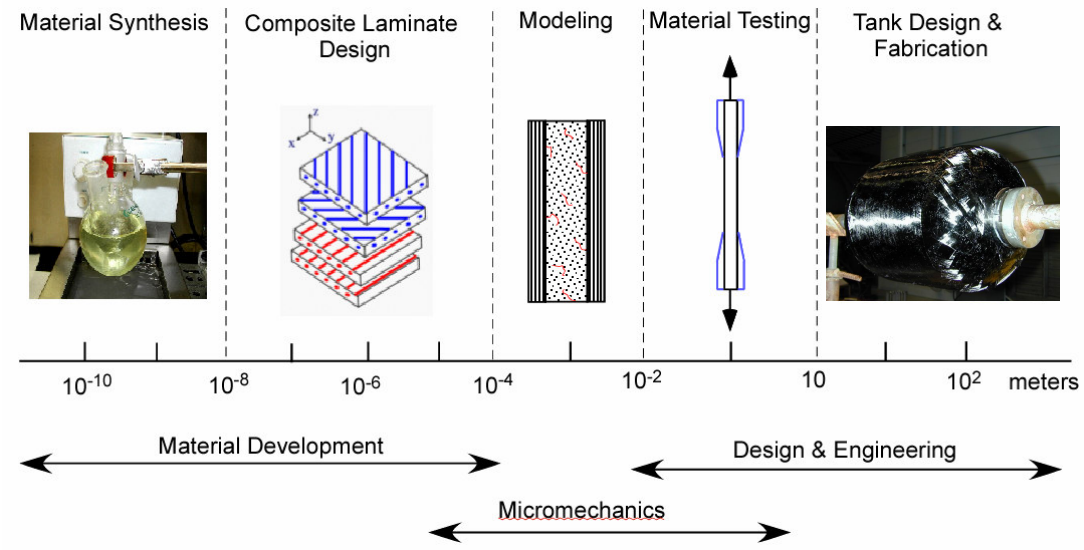

Figure 2. The *integrated systematic approach* provides an inter-disciplinary and multi-scale methodology in developing lightweight linerless composite tanks.

to develop linerless composite tanks have met with limited success due to a lack of focus across all relevant areas and size scales.

II. Material Development

A. Development of Novel Matrix Materials

CTD's material development effort towards linerless composite tanks has focused on toughened epoxy matrices with improved resistance to microcrack formation. Several new approaches have been investigated in novel material formulation, including the use of rubbers and commercially available block copolymer impact modifiers. During the material development effort, epoxy resin mixtures have been selected to achieve an optimized balance between resin cost, performance, and processing. In addition, various curing agents have been evaluated to provide improved pot-life and shelf-life with a room temperature cure. Longer pot-life times are anticipated to enable fabrication of larger-scale composite structures and provide for a higher level of end-user acceptability.

CTD has also used vapor grown carbon fiber (VGCF) nano-reinforcements in the matrix for improved modulus and higher inter-laminar shear strength at the ply interfaces. Experimental results indicate that the microcrack resistance of cross-ply laminates made with VGCF reinforced epoxy matrix is significantly higher than that of commercial-off-the-shelf (COTS) materials like Cytec's 977-2 and 977-3 used traditionally in composite tanks.

B. Microcracking Performance Assessment through Uniaxial Tests

'Microcracking fracture toughness' (MFT) has been identified as an effective analytical tool to screen and down-select the materials for linerless composite tanks.[3-6] The instant of formation of the microcrack is predicted when the total energy released by the formation of that microcrack reaches the critical energy release rate for microcracking, G_{mc}, or the MFT. Evaluating a material's MFT involves uni-axial tensile tests of cross-ply laminates $[0/90_n]_s$ where n is the number of plies in the 90^o plies sandwiched between the 0^o plies (see Figure 3). Laminates for MFT tests were manufactured by CTD using a wet lay-up procedure and a high-temperature hydraulic press for compaction and cure resulting in a fiber volume fraction of $V_f = 60\%$. Test specimens (13 mm wide by 200 mm long) are cut from the laminate using diamond saw and edges polished by a 3 micron diamond slurry. Typical ply thickness of a specimen is 0.15 mm.

During the MFT test, the specimen is subjected to tensile strain, which is increased in increments. The edge of the specimen is inspected at each strain increment using a 10x hand-held digital microscope connected to a personal.

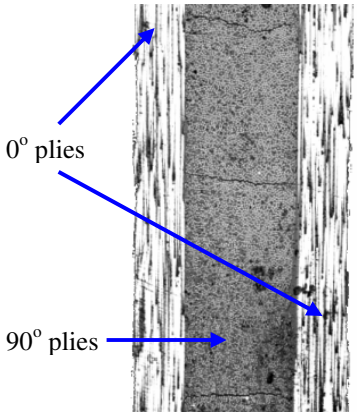

Figure 3. The polished edge of a MFT test specimen of $[0/90]_s$ layup.

The number of microcracks in the central ply is counted on the computer monitor while the microscope traverses the length of the specimen edge. The microcrack count is performed for each edge of the specimen and the average microcrack density (number of microcracks divided by the specimen edge length) is reported for each strain level. The procedure is repeated until the tensile failure of the specimen is complete. Determining the microcrack density of the specimens in situ in the test frame avoids dismantling the specimens from the testing machine and remounting them under an optical microscope for counting of microcracks. More importantly, microcracks are easily identified and more accurately counted when the specimen is strained, since previous researchers have reported closure of microcracks in the absence of load.

Figure 4 shows the microcrack density as a function of the applied strain for several different composite materials tested at room temperature. The laminate configuration for these specimens was $[0_2,90_4]_s$ with a ply thickness of 0.15mm and a fiber volume fraction of 60%. The higher the microcrack fracture toughness of a material, the lower the microcrack density at a given strain level, which in turn is likely to promote less permeation of fluids through the tank wall. From these test results, several of CTD's new matrix materials (e.g., CTD-7.1 and CTD-DP5.1) show very high microcrack fracture toughness as compared to the industry standard Cytec 977-2 and 977-03 resins.

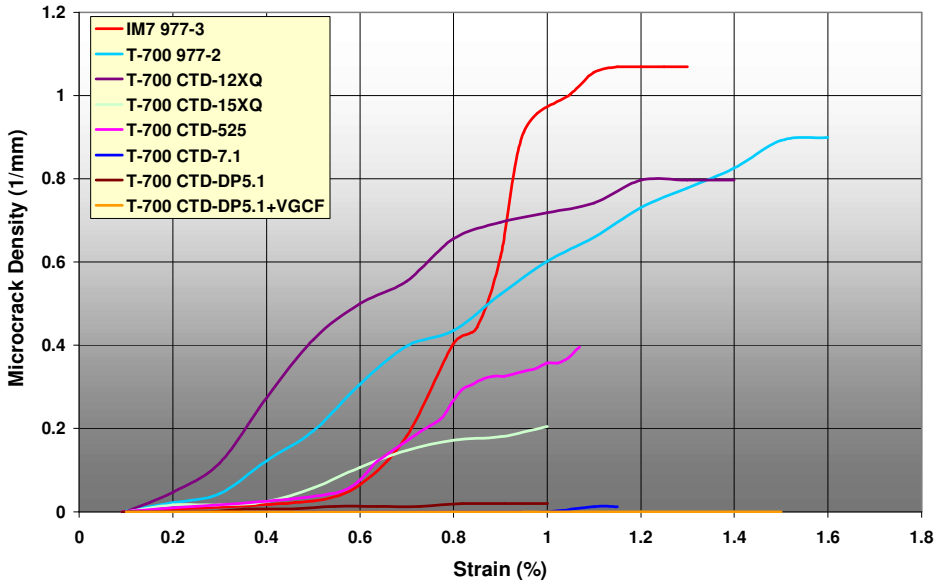

Figure 4. Growth of microcracks vs. strain in a cross-ply laminate for several materials tested by CTD at room temperature.

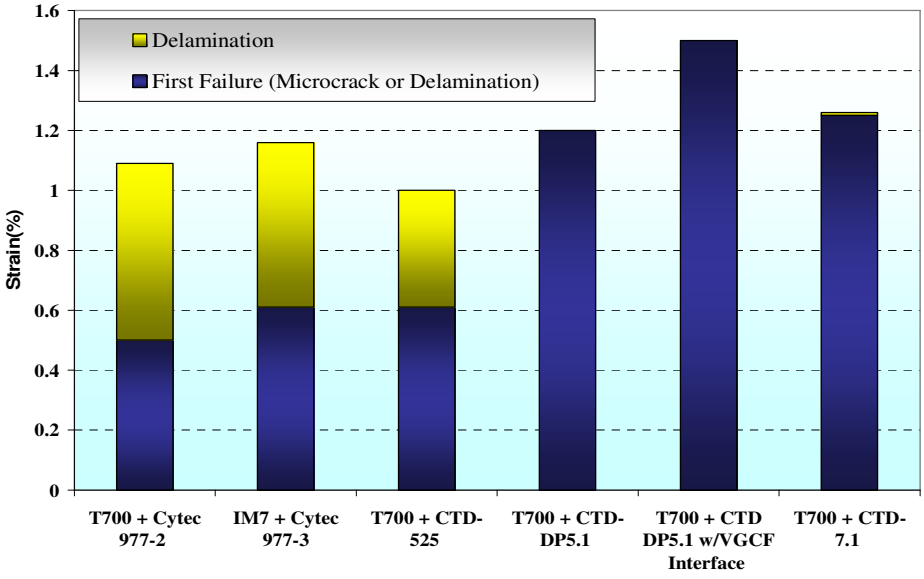

Figure 5. Strain to initiate microcracking and delamination for several materials tested at room temperature.

The strains to initiate microcracking and delamination are important design parameters for linerless composite tanks. Figure 5 shows these two types of failure strains in cross-ply laminates for several materials tested by CTD at room temperature. Results shown in this plot are averaged over five different specimens. It is interesting that no microcracks are detected in specimens made with CTD DP5.1 and CTD 7.1. The first mode of failure was delamination in these materials that occurred above 1% strain, a target strain level to achieve the design optimization goals for linerless composite tanks.[6] Addition of nano-reinforcements in the form of vapor grown carbon fibers (VGCFs) in the ply interface increased the delamination strain to 1.5%. This matrix-driven failure

mode of the material is encouragingly close to the ultimate fiber-failure strain of 1.7%. This is a significant performance improvement in comparison to Cytec's 977-2 and 977-3 materials that show microcrack formation at strain levels close to 0.5%.

C. Permeability Performance Assessment through Sub-Component Biaxial Pressure Tests

The MFT tests described above are designed to screen the matrix materials based on their performance against microcrack formation under uniaxial load. In addition to these coupon-level tests, a sub-component-level test is required to characterize permeability performance of composite laminates subjected to biaxial stress under pressure loading. This test characterizes laminates fabricated by a method that represents the actual fabrication of the composite tanks. Hence, the results of the tests should directly relate to full-scale tank performance.

A schematic of the test setup being developed by CTD is shown in Figure 6.[7] The test article consists of a filament-wound, linerless composite pipe with adhesively bonded metallic end sleeves (Figure 7(a)) and flanged end caps enclosed in a vacuum chamber that suspends the cylinder by one end (Figure 7(b)). The unsupported end of the test cylinder is free to expand, thus achieving the desired 2-to-1 ratio in hoop-to-axial stress, which is typical of cylindrical pressure vessels. A vacuum pump and helium leak detector are attached to the vacuum chamber to measure the rate of helium leakage as a function of pressure and temperature. The objective of the test is to measure the helium permeation as well as the hoop and axial strains in the pipe as a function of the applied pressure and the progressive damage due to microcracking in the composite plies. The test results will be used to validate the analytical predictions of permeability and ultimate strength based on micromechanics as explained in the following section.

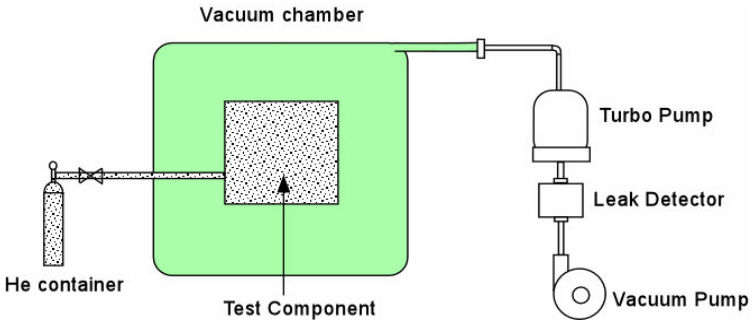

Figure 6. Schematic design of the permeability test setup.

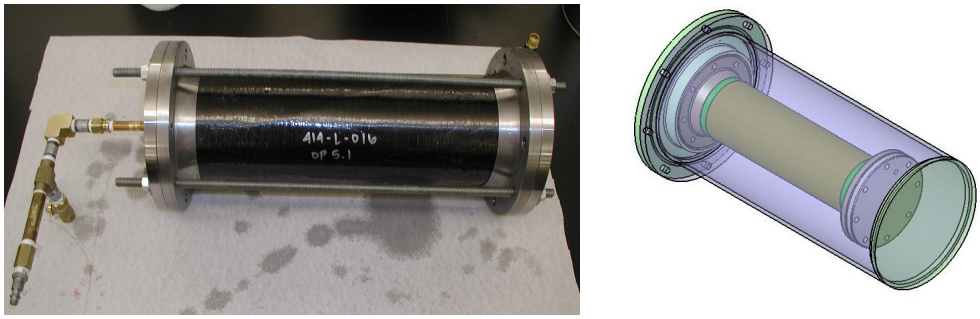

(a) **(b)**

Figure 7. Test fixture for pressure testing of filament wound pipes.

III. Micromechanics

In composites, failure is usually a progressive process. Often, a wide margin can be found between the first incident of micro-scale failure and the ultimate failure. Indeed, the accumulation of damage through microcracking is such a progressive failure process, and understanding this failure progression and the effect of microcracking on permeability are keys to the design optimization of linerless tanks. As depicted in Figure 8, permeation pathways can

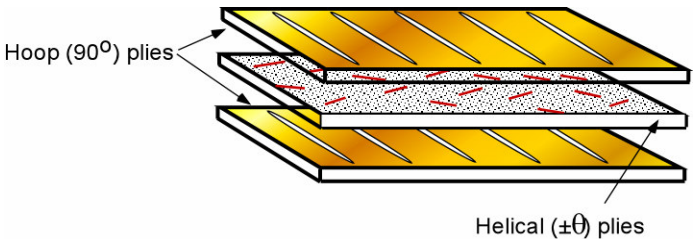

Figure 8. Idealization of leakage path through microcracks in adjacent plies of a composite laminate.

develop through microcracks in adjacent layers of a multi-layer, filament-wound tank. The goal of the micromechanics-based analysis is to establish analytical models predict the nucleation and growth of microcracks and relate the microcrack density to global stiffness reduction and ultimately to leakage.

A. Microcracking and Permeation

The successful design optimization of a linerless tank requires an understanding of the degree of microcracking in the individual plies and how that affects the permeation or flow of fluid through the laminate.[8] The laminate in a filament-wound composite tank typically consists of interspersed layers of hoop and helical plies. Therefore, the cylindrical section of the tank shell can be modeled as a sequence of mixed ply laminates $[90/(\pm\theta)]_s$ stacked in series; angles being measured with respect to the cylinder axis. As the tank is pressurized, equilibrium dictates that the ratio $\sigma_\theta / \sigma_a = 2$ remains constant in the cylinder section, where σ_θ is the hoop stress and σ_a is the axial stress. Since the helical plies are subjected to a higher transverse stress magnitude of $\sigma_\theta = 2\sigma_a$, they will experience microcracking before the hoop plies.

The expected evolution of microcrack density in the composite laminate is illustrated schematically in Figure 9(a). Because of the biaxial stress state, analytical estimation of the growth of microcracks needs to be performed ith the constraint of $\sigma_\theta = 2\sigma_a$ (Figure 9(b)).[6] As long as microcracking does not occur in the hoop plies, they can prevent the flow of fluids through the laminate, thereby keeping the permeability of the laminate negligible. However, as the pressure is further increased, a critical value of internal pressure p_c (and the corresponding axial stress, σ_a) is reached that causes microcracking in the hoop plies, thereby providing an interconnected pathway for the fluid to permeate through the entire laminate. The following section illustrates how the critical pressure p_c can be estimated using the MFT of the matrix material.

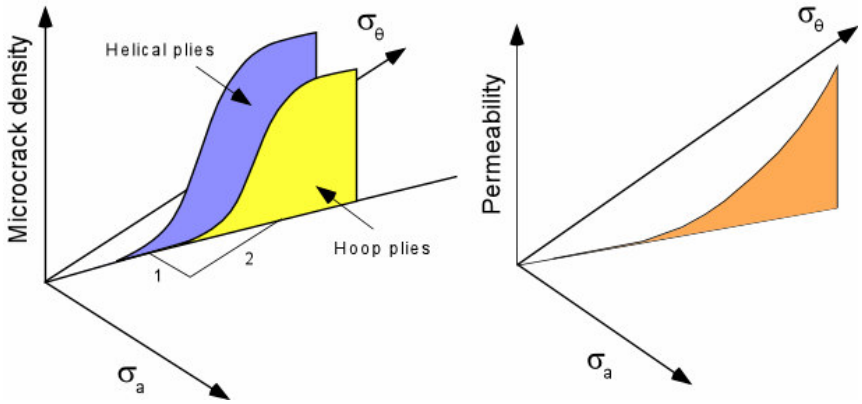

Figure 9: Growth of (a) microcracks and (b) permeability in a composite laminate under biaxial load.

B. Prediction of Microcrack Initiation under Biaxial Load

Containment and 'management' of microcrack-induced damage in the linerless composite tank requires the ability to predict microcrack initiation in a multi-ply laminate subjected to biaxial loading, taking full account of both anisotropy and thermally induced stresses. Figure 10 shows the cylindrical section of a filament-wound tank subjected to a biaxial stress. The tank is assumed to have closed ends, thereby producing an axial stress $\sigma_a = pR/2t$ and a circumferential stress $\sigma_\theta = pR/t$, where p is the internal pressure, R is the tank radius and $t = 2(t_1 + t_2)$ is the total thickness of the laminate. Tracking the damage evolution in the laminate

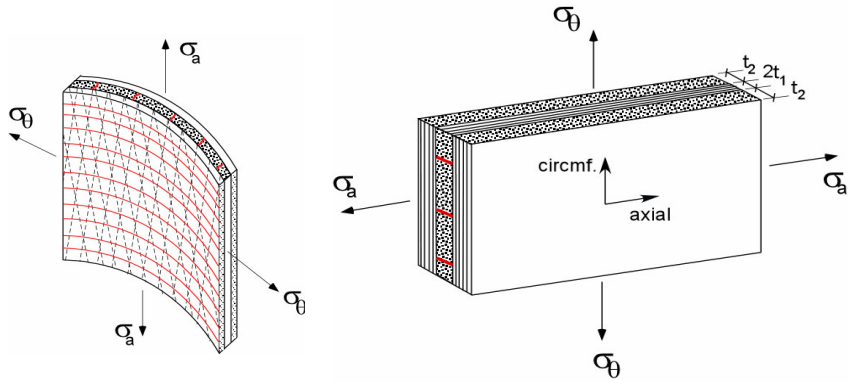

Figure 10. Biaxial stresses acting on (a) a tank cylindrical section and (b) an idealized geometry.

due to internal pressurization will require solving two simultaneous equations for the two directions – axial and circumferential. The damage evolution laws for the biaxial loading conditions are derived in Appendix A. These equations require an analytical understanding of the degradation of the effective stiffness and coefficient of thermal expansion of the laminate in the two directions due to the evolving damage in both the hoop and helical plies.

If the tank is fabricated with a room-temperature-cure resin system, like CTD 7.1, and operated at room-temperature, the differential between the stress free temperature during tank cure and the tank test temperature can be neglected, i.e. $\Delta T \approx 0$. Substituting $\sigma_a = pR/2t$ and $\sigma_\theta = pR/t$ in equation A2 (see Appendix A), the pressure p at which microcracks are initiated in the hoop plies is derived as:

$$p = \frac{2t}{R(1+2k_a)}\sqrt{(2G_{mc}D^{90})\left\{\frac{1}{E_a(D^{90})}-\frac{1}{E_a}\right\}} \tag{1}$$

where, G_{mc} is the microcrack fracture toughness of the composite material, $D^{90} = 1/(2\rho t_1)$ is the microcrack density and $\rho = a/t_1$ is the normalized microcrack spacing in the hoop (90^o) plies. The parameter k_a is a laminate constant that has been defined in Appendix A. E_a is the effective modulus of the laminate in the axial direction that depends on the microcrack density D^{90} in the hoop plies. Assuming $\theta \approx 0$ for low-angle helical plies typical of a filament-wound tank, the functional dependence of E_a on the microcrack density D^{90} can be derived as:[9]

$$\frac{1}{E_a(D)} = \frac{1}{E_a} + \frac{4t_1^{\,2}C_3E_2^{\,2}}{tE_a^2}\chi(D^{90})D^{90} \tag{2}$$

where the parameter C_3 is a material constant that has been defined elsewhere in reference to the theoretical framework of microcrack fracture toughness.[6]

Combining eqs. (1) and (2), the engineering estimate of the critical pressure p_c at which microcracks are initiated in the hoop plies under biaxial load is derived as:

$$p_c = \frac{2t}{R(1+2k_a)}\left(\sqrt{\frac{G_{mc}tE_a^{\,2}}{2t_1^{\,2}C_3E_2^{\,2}\chi(D)}}\right) \tag{3}$$

The material's MFT (G_{mc}) measured from uniaxial experiments can therefore be used in eq. (3) to predict the critical pressure where the tank starts to leak.

C. Dependence of Permeability on Damage Evolution

Initiation of leakage is not catastrophic in composite tanks as long as it is contained within engineering design limits. Therefore, in some cases it may be necessary to predict the leakage or permeability of the tank laminate beyond the critical pressure where the permeability becomes non-zero. The concept of effective conductance can be used to estimate the leak rate of the fluid through the composite laminate.[10] Effective conductance of the laminate is directly related to the volumetric flow rate of the fluid leaking through a composite laminate and is defined by:

$$\overline{C} = \frac{Q}{\Delta P} \tag{4}$$

where Q is the flow rate and ΔP is the pressure differential across the laminate. If C_1, C_2, …C_n define the individual conductance of each ply junction, the effective conductance of the composite laminate can be defined as:[10]

$$\overline{C} = \left[\sum_{k=1}^{n}\left(\frac{1}{C_k}\right)\right]^{-1} \tag{5}$$

Now, if the adjacent plies of the tank laminate are microcracked, the conductance of each ply junction can be hypothesized to be:

$$C_k = \xi \frac{\omega_k \omega_{k+1} \Delta_k \Delta_{k+1}}{\cos\theta_k} \tag{6}$$

where ξ is a material constant to be determined from experiments, ω_k is a parameter that defines the damage, Δ_k is the mean-opening displacement of the microcracks in the k^{th} ply and θ_k is the angle of the helical ply, measured with respect to the tank axis. Combining Equations (4)-(6), the effective mass flow rate through a microcracked laminate is given by:

$$Q = \xi \left[\sum_{k=1}^{n} \left(\frac{\cos\theta_k}{\omega_k \omega_{k+1} \Delta_k \Delta_{k+1}} \right) \right] \Delta P \tag{7}$$

The average microcrack opening displacement (MCOD), Δ depends on the degradation in effective stiffness of the composite ply and can be calculated from the reduction in elastic modulus of the laminate. Computations show that MCOD increases with the crack spacing and decreases with microcrack density. [11]Analytical expressions for the MCOD in the 90^o plies of a $[(\pm\theta)/90]_s$ laminate as a function of microcrack density is given in Appendix B.

Analytical estimation of Δ in each ply and its subsequent incorporation in eqn. (7) completes the theoretical formulation relating the flow rate Q of a multi-ply composite tank laminate as a function of applied internal pressure, P. The formulation can be implemented in the finite element analysis of a linerless composite tank to predict the permeability of the entire tank.

IV. Tank Design and Engineering

D. Isostrain Design to Minimize Microcracking in Domes

Traditionally the domes in composite pressure vessels have been designed based on netting analysis.1 For filament-wound tanks such optimized dome designs are also referred to as *geodesic isotensoid* designs. The word *geodesic* refers to a curvature that provides stability against fiber slippage during winding and the word *isotensoid* refers to a structurally optimized dome contour that ensures uniform tension along the fiber direction on any point of the dome. Essentially, the structural design of an isotensoid dome neglects the failure mode of the composite transverse to the fiber direction. The philosophy of isotensoid domes is adequate for a lined pressure vessel where the liner is responsible for fluid containment and therefore, matrix microcracking is not an influencing factor. The structural design of a dome in a linerless composite tank, on the other hand, must account for the failure characteristics of the composite transverse to the fiber.

An *isostrain* dome profile is an alternative design, which assures that the fibers are placed along the directions of the principal stresses in each layer and that the principal strains are constant at any point of the dome. As matrix microcracking has been shown to be a strain-dependent failure phenomenon, it follows that an isostrain dome design will provide more uniform microcracking performance, and hence, a more efficient design to inhibit microcracking and permeation than an isotensoid design. The fundamental assumptions and topology of an isostrain dome profile are discussed in Appendix D and a comparison of isostrain and isotensoid dome profiles is shown in Figure 11. In this derivation it is shown that the ratio of the stress in the fiber direction to that in the transverse direction at any point on the dome is a constant, *k,* defined in eqn. (9). Note that the isotensoid design is essentially a degenerate case of the

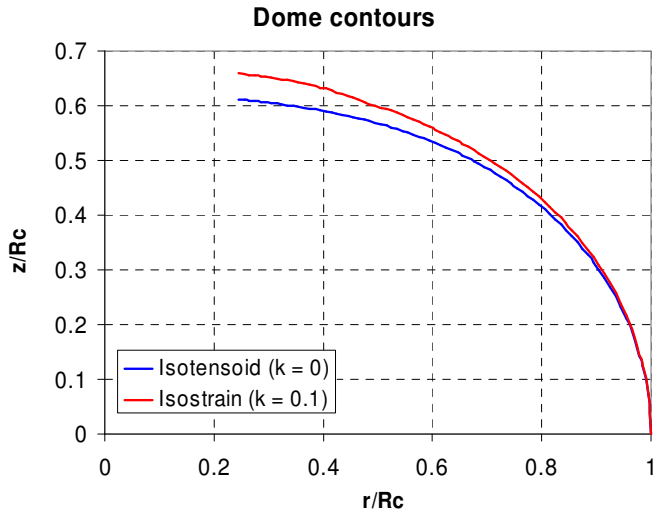

Figure 11: Comparison of an isotensoid and an isostrain dome profile

isostrain design in which k is zero.

$$k = \sigma_2 / \sigma_1 \tag{8}$$

If the material is assumed to be linearly elastic, as most carbon fiber reinforced thermosets are, the above relation will hold true when the shell is pressurized until one of the stresses σ_1 or σ_2 attains the maximum value or the maximum strength. Assuming that the strength of a uni-directional ply is defined by σ_1^u and σ_2^u in the two directions, parallel and perpendicular to the fiber, a material constant, k_1, which relates these orthotropic failure stresses can be defined:

$$k_1 = \sigma_2^u / \sigma_1^u \tag{9}$$

Figure 12 shows the different laminate response when the dome is pressurized for different values of the operating stress ratio, k, relative to the material strength ratio, k_1. An assumed failure envelope of the unidirectional ply is defined by the rectangle, $\sigma_1 = \sigma_1^u, \sigma_2 = \sigma_2^u$. The three lines consider three hypothetical cases depending on the material characteristics. Line 1 characterizes the case when $k > k_1$ and the matrix fails in the tank dome before the fiber ruptures. Line 3 represents the case when $k < k_1$, when the fiber fails in the dome before the matrix. The ideal case is shown in Line 2 where $k = k_1$ and the matrix and the fiber fail simultaneously.

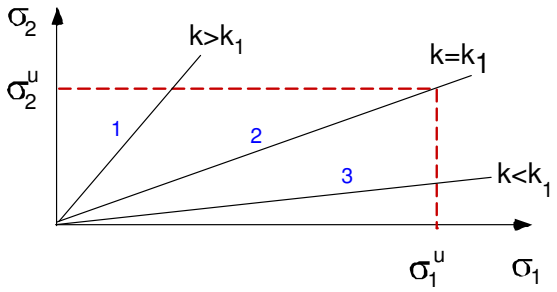

Figure 12: Failure envelope and types of loading for a composite shell.

E. Finite Element Analysis of Filament-Wound Tanks

In order to accurately account for the multiple aspects of material performance (i.e., orthotropic strength, changing stiffness, permeability, etc.) the structural design of the linerless composite tank must refined using Finite Element Analysis (FEA). A proprietary in-house program has been developed by CTD to generate the finite element model of the composite tank given a user-defined envelope of the tank geometry, the design parameters, and the tank's laminate sequence. The program creates an input file to be interpreted by a commercial finite element program, like ABAQUS.

An axisymmetric model for half of a prototype 10" ID x 18" long tank created by this program is shown in Figure 13. The FEA model accounts for:

1. Spatially varying material properties in the tank structure
   - The orthotropic properties of the composite layers in the filament wound cylindrical shell
   - The orthotropic properties and thickness of each element in the dome
   - The polar buildups during wind
   - The hoop stagger at the transition region
2. Geodesic isostrain (or isotensoid) dome profile.
3. The non-linear variation of material properties (elastic moduli, CTEs) with strain level, degree of microcracking, temperature etc.
4. Interface between the polar bosses and the composite shell overwrap
5. Load sequence that can combine pressure and thermal loads.

The boundary conditions applied to the model consist of symmetry conditions at the cut surface in the middle of the cylinder, a uniform pressure of p on the inside surface of the tank as shown in Figure 13, and a displacement boundary condition ($u_y = 0$) is imposed on the center of the tank ($y = 0$) to restrain it against rigid body motion in the axial direction. The interface between the composite shell and the polar boss is modeled using ABAQUS's "cohesive elements" (Figure 14). These elements are effective in modeling the behavior of adhesive joints, interfaces in composites, and other situations where the integrity and strength of interfaces may be of interest.[12] The constitutive response of these elements is assumed to be based on a traction-separation description of the interface. The behavior of the interface prior to initiation of damage is described as linear elastic. Once the damage is initiated, the stiffness degrades under tensile and/or shear loading, but is unaffected by pure compression. A simple linear damage evolution law is used to describe the rate at which the material stiffness of the interface is degraded once the pre-defined damage initiation criterion is reached.

The finite element analysis is performed using a non-linear geometry option with the internal pressure applied incrementally in time steps up to the design pressure. Figure 15 plots the longitudinal and transverse strain of each ply along the meridional distance (distance measured along the tank meridian / dome profile) starting from the center of the tank. Figure 15(a) also shows that there are no stress peaks in the dome regions that would cause a dome rupture if the pressure was increased beyond its design pressure. However Figure 15(b) shows that the transverse strain is abnormally high in the hoop plies around the cylinder-to-dome transition area. This is likely to cause microcracking in the hoop plies leading to leakage in the cylinder-to-dome transition area. This is precisely the level of insight that is necessary to refine the laminate and shell design in order to maximize efficiency.

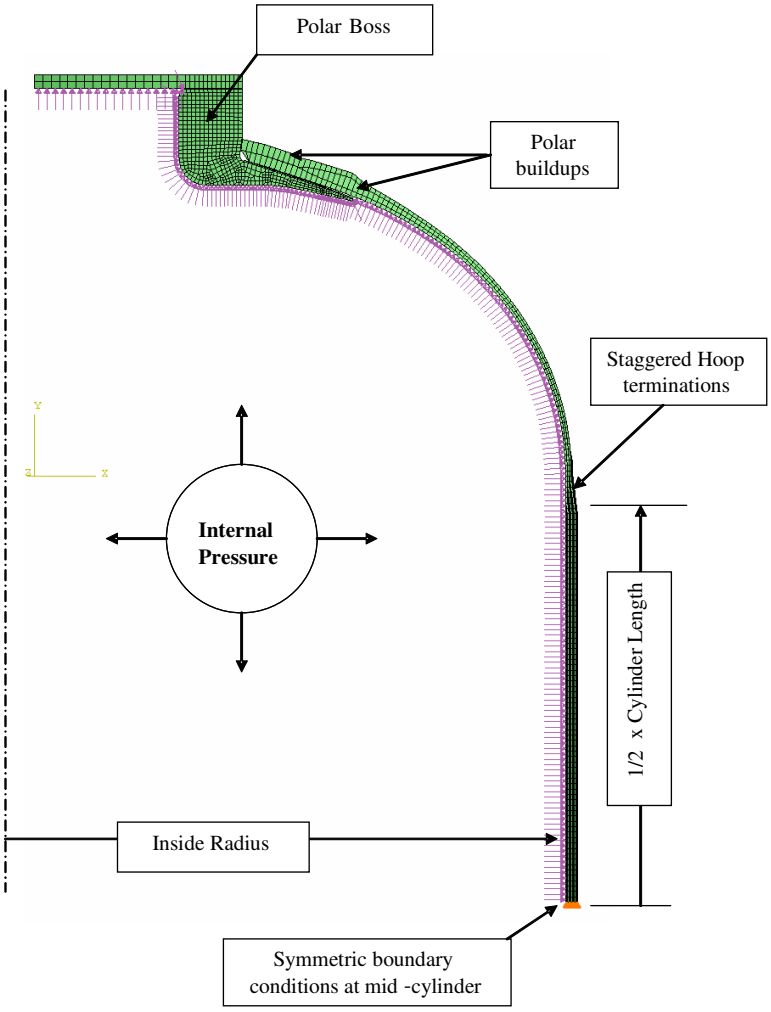

Figure 13: FEA model of a filament wound composite tank

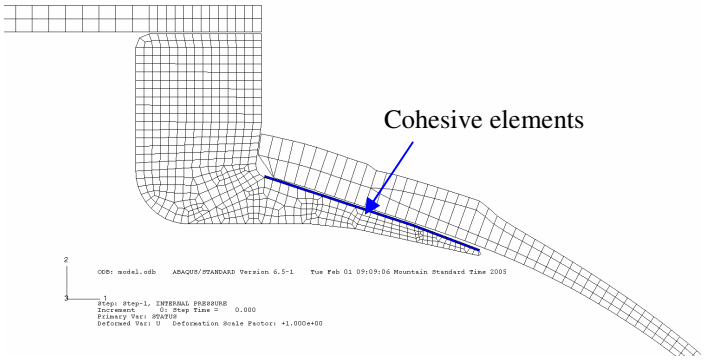

Figure 14: ABAQUS's cohesive elements are used to model the interface between polar boss and composite overwrap.

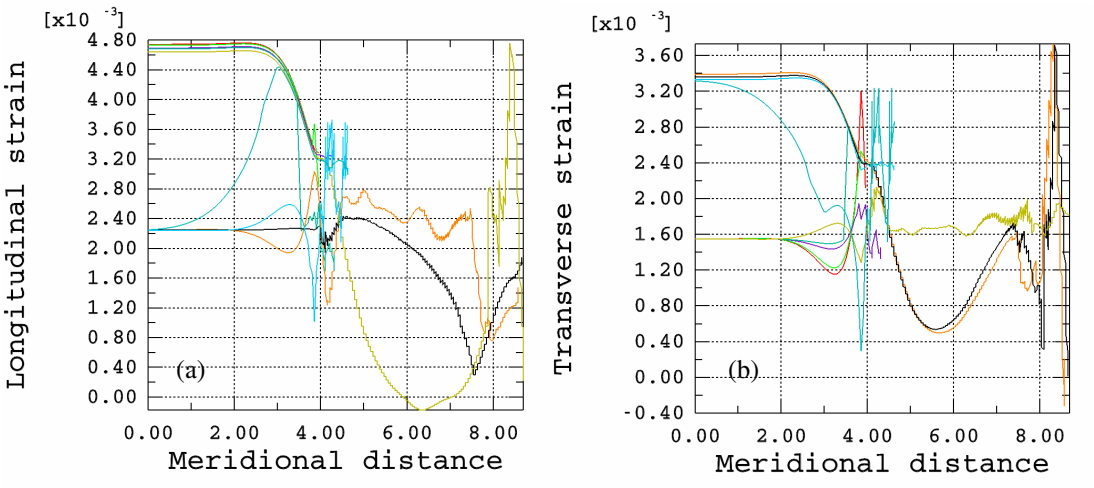

Figure 15: (a) Longitudinal and (b) Transverse strain in composite plies of the prototype tank at its operating pressure derived from FEA analysis

F. Fabrication of Prototype Linerless Composite Tanks

Prototype linerless composite tanks, 10-inch diameter x 18-inch, were fabricated using a 5-axis filament winding machine at the Air Force Research Laboratory, Kirtland. The mandrel was fabricated in two halves using a washable eutectic salt called AquaPour™ made by Advanced Ceramics Research, Inc., Tucson, Arizona. Four tows of Toray T700-SC 12K carbon fiber tows and a toughened epoxy CTD 7.1 resin were used during the fabrication process (Figure 16). The tank laminate layup consisted of interspersed hoop and helical layers, with the hoop layers providing compaction and consolidation of the previous helical layer. The winding tension was varied to avoid fiber microbuckling. Finished tanks were oven cured, after which the mandrels were washed out using water leaving the finished linerless composite tanks. At the time of the present report, CTD was preparing to perform pressure testing on these prototype tanks.

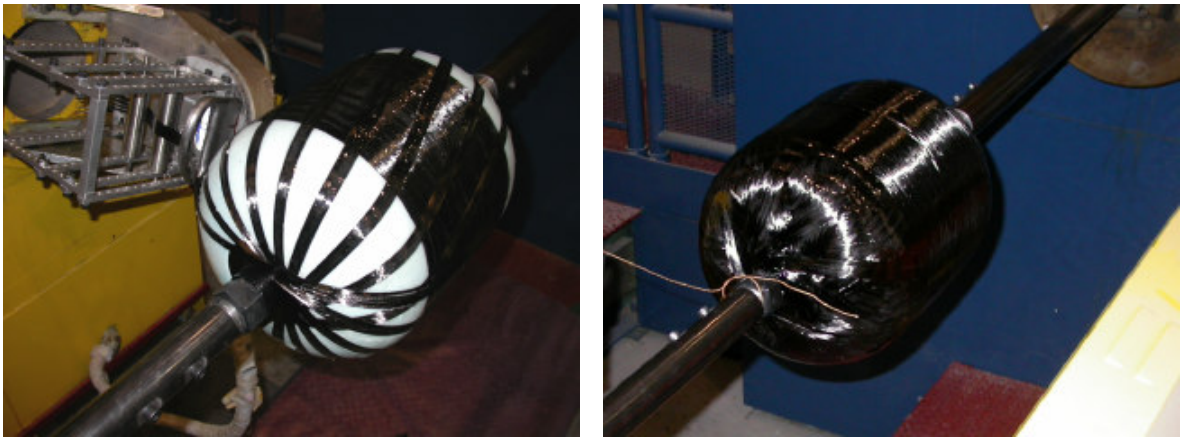

Figure 16: Different stages in the fabrication of a prototype linerless composite tank

Summary

This paper describes a program currently underway at Composite Technology Development, Inc. to dramatically improve the design and capabilities of lightweight linerless composite tanks. The program integrates material development and characterization, micromechanics-based analyses, and structural design and fabrication of prototype tanks. This *integrated systematic approach*, addresses the multi-scale and multi-disciplinary issues that are critical to linerless composite tank design by looking concurrently at material requirements capabilities and tailoring, refinement of fabrication process, and structural design optimization. Unlike traditional composite over-wrapped pressure vessels, linerless composite tanks depend on the composite shell itself to serve as a permeation barrier in

addition to carrying all pressure and environmental loads. Designing these tanks requires accurate knowledge of the structural response of the tank on the macro-scale as well as the material behavior on the micro-scale.

It is clear that limiting and managing the development of microcracks and microcrack-induced permeability in the composite shell dictates that new materials must be tailored specially for this purpose. To that end, this paper describes how micromechanics-based analysis is used to: 1) define critical material-performance parameters that drive the development of new toughened matrices, and 2) predict microcrack formation and permeability in composite laminates under biaxial load. Test data are presented that show new toughened resin systems exhibit dramatic improvements in microcrack fracture toughness, and strain-to-failure response as compared to industry-standard epoxy systems. The concept of *isostrain* design is introduced for use in optimization of dome structural design. Issues related to finite element analysis of these tanks are discussed, and a proprietary computer program to generate the finite element model of a composite tank given a user-defined envelope of the tank geometry, the design parameters, and the tank's laminate sequence, is described. Finally, the paper presents progress to date in designing and fabricating linerless composite tanks using a newly developed, microcrack-resistant resin system.

Appendix A. Damage Evolution in a Tank Laminate Under Biaxial Load

The cylindrical section of a filament-wound composite tank consists of interspersed layers of hoop and helical plies subjected to a biaxial stress state. Consequently, the building block for damage (microcrack) analysis of the laminate consists of a $[90/(\pm\theta)]_s$ laminate for circumferential load (σ_a) and a $[(\pm\theta)/90]_s$ laminate for the axial load (see Figure 17). For the former, the damage evolution law in the helical ($\pm\theta$) ply of the $[90/(\pm\theta)]_s$ laminate is given by:[13]

$$\sigma_\theta + k_\theta \sigma_a = \sqrt{\frac{2G_{mc}D^{\pm\theta}}{\left\{\frac{1}{E_\theta(D^{\pm\theta})} - \frac{1}{E_\theta}\right\}}} - \frac{\alpha_\theta(D^{\pm\theta}) - \alpha_\theta}{\left\{\frac{1}{E_\theta(D^{\pm\theta})} - \frac{1}{E_\theta}\right\}}\Delta T \tag{A1}$$

Similarly, the damage evolution law in the 90° plies of the building block defined by $[(\pm\theta)/90]_s$ laminate is given by:

$$\sigma_a + k_a \sigma_\theta = \sqrt{\frac{2G_{mc}D^{90}}{\left\{\frac{1}{E_a(D^{90})} - \frac{1}{E_a}\right\}}} - \frac{\alpha_a(D^{90}) - \alpha_a}{\left\{\frac{1}{E_a(D^{90})} - \frac{1}{E_a}\right\}}\Delta T \tag{A2}$$

where, G_{mc} is the microcrack fracture toughness of the composite material, D^{90} and $D^{\pm\theta}$ are the damage variables for the hoop (90°) and helical (±θ) plies, E_θ and E_a are the moduli, α_θ and α_θ are the effective coefficients of thermal expansion (CTE) of the tank laminate along the circumferential and axial direction, ΔT is the difference between the stress-free temperature of the laminate (cure temperature) and the test temperature and k_θ an k_a are laminate constants defined as:[13]

$$k_\theta = \frac{\frac{E_\theta}{E_a}\nu_{21}^{\pm\theta} - \nu_{\theta a}}{1 - \nu_{\theta a}\nu_{21}^{\pm\theta}}; k_a = \frac{\frac{E_a}{E_\theta}\nu_{21}^{90} - \nu_{a\theta}}{1 - \nu_{a\theta}\nu_{21}^{90}} \tag{A3}$$

The transcendental set of equations (A1) and (A2) together define a complete description of damage evolution in the tank laminate with the help of microcrack fracture toughness and an apriori knowledge of the change in effective modulus and effective CTE of the laminate in both the circumferential and axial directions.

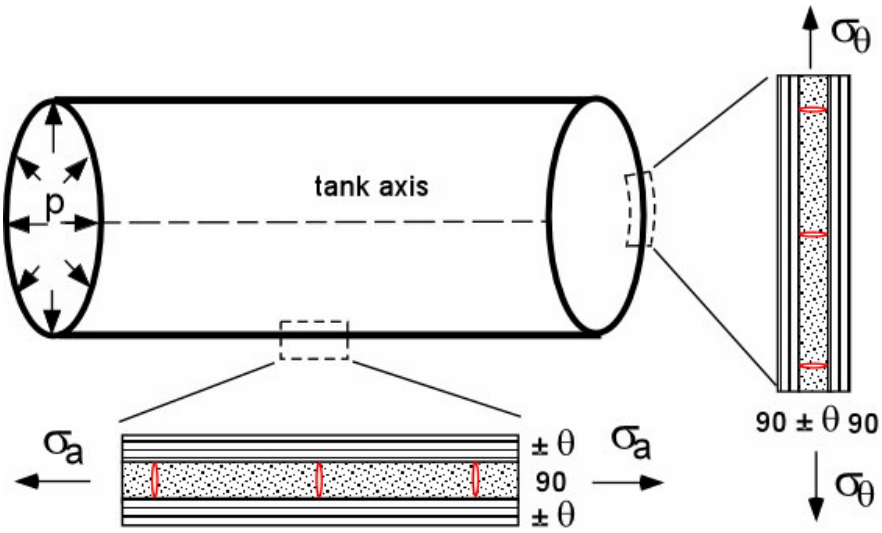

Figure 17: Two complimentary building blocks for damage analysis of a filament wound tank.

Appendix B. Modulus Reduction Due to Microcracks in the Hoop (90°) Plies

The expression of the effective elastic modulus E of the $[(\pm\theta)/90]_s$ laminate as a function of microcrack density in the 90° plies, normalized with respect to the modulus E_0 of the virgin laminate is given by:[14,15]

$$\frac{E}{E_0} = \frac{1}{1 + aD^{90}\chi(\rho)} \tag{B1}$$

where:

$$a = \frac{E_2 t_1}{E_x^{\theta} t_2}\left(\frac{1-\nu_{12}\nu_{xy}^0}{1-\nu_{12}\nu_{21}}\right)\left(1+\nu_{xy}^{\theta}\frac{S_{xy}^{\theta}t_1 + S_{12}t_2}{S_{yy}^{\theta}t_1 + S_{11}t_2}\right) \tag{B2}$$

$$\chi(\rho) = 2\alpha\beta\left(\alpha^2+\beta^2\right)\frac{\cosh 2\alpha\rho - \cos 2\beta\rho}{\beta\sinh 2\alpha\rho + \alpha\sin 2\beta\rho} \tag{B3}$$

In (B1), (B2) and (B3) D^{90} is the microcrack density in the hoop (90°) plies, $\rho = 1/\left(2D^{90}t_1\right)$ is the normalized crack spacing, S_{ij}^{θ} represents the compliance terms for the ±θ ply and ν_{xy}^0 and S_{ij} represent the Poisson's ratio and the compliance terms respectively for the virgin $[(\pm\theta)/90]_s$ laminate.

Figure 18 plots the reduction in effective modulus of a $[(\pm\theta)/90]_s$ laminate defined by eqn B1 for three different values of θ. The ply thickness used in computation is 0.15 mm and the values of θ selected are typical of a composite tank fabricated by CTD.

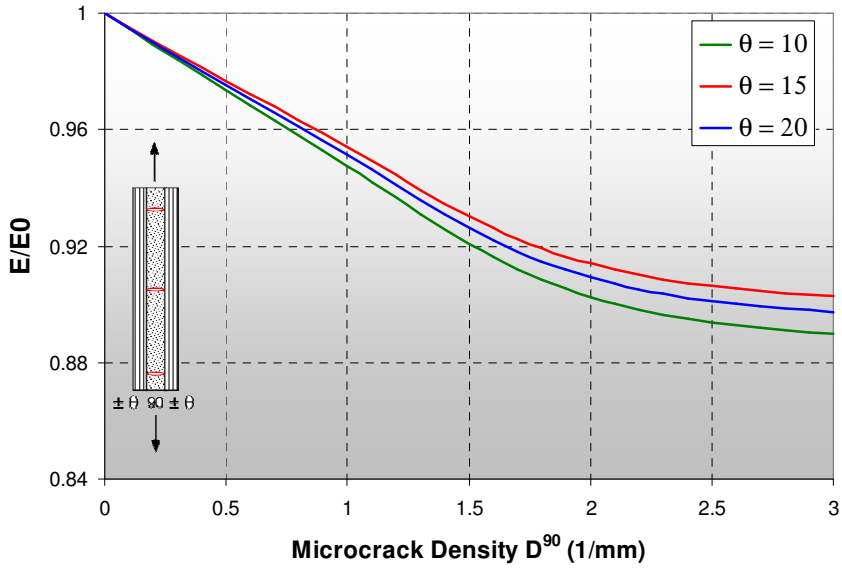

Figure 18: Reduction of the effective modulus of a $[(\pm\theta)/90]_s$ laminate with increase in microcrack density D^{90} in the 90^o plies

The average microcrack opening displacement (MCOD) in the 90^o ply can be computed from:[14]

$$\Delta = t_1 \bar{\varepsilon}\chi(\rho)\frac{E_2 t_1}{2E_x^{\theta} t_2}\left(\frac{1-\nu_{12}\nu_{xy}^0}{1-\nu_{12}\nu_{21}}\right)\left[1+\frac{S_{22}t_1}{S_{xx}^{\theta}t_2}-\frac{\left(S_{xy}^{\theta}t_1+S_{12}t_2\right)^2}{S_{xx}^{\theta}t_1\left(S_{yy}^{\theta}t_1+S_{11}t_2\right)}\right] \tag{B4}$$

Appendix C. Modulus Reduction Due to Microcracks in the Helical (±θ) Plies.

Assuming that during the initial stages of loading, microcrack formation in the angle-ply (±θ) laminate is dispersed and random, the reduction in ply elastic parameters due to dispersed microcracks can be modeled using mean field theories of elasticity. The formation of microcracks in the angle-ply (±θ) layer can be modeled as formation of multiple slits in an orthotropic 2-D medium, in which all slits are divided into two systems. Each of these two-slit systems consists of *N/2* aligned microcracks of equal length 2a. Microcracks in these two systems subtend angles $+\theta$ and $-\theta$, respectively. The elastic parameters E_{11} and E_{22} of the ply can be computed by solving the following linear equations:[16]

$$\begin{aligned}\left(1-2\pi\omega B_{11}\right)\frac{1}{E_{11}}-2\pi\omega B_{12}\frac{1}{E_{22}}&=\frac{1}{E_{11}^0}\\ -2\pi\omega B_{11}\frac{1}{E_{11}}+\left(1-2\pi\omega B_{22}\right)\frac{1}{E_{22}}&=\frac{1}{E_{22}^0}\end{aligned} \tag{C1}$$

where,

$$\begin{aligned}B_{11}&=1-2\cos^2\theta+2\cos^4\theta-\cos^6\theta\\ B_{12}&=\cos^2\theta-2\cos^4\theta+\cos^6\theta\\ B_{21}&=\cos^2\theta-\cos^8\theta-\sin^6\theta\cos^2\theta\\ B_{22}&=\cos^8\theta+\sin^6\theta\cos^2\theta\end{aligned} \tag{C2}$$

and $\omega = Na^2$ is the Budiansky and O'Connell microcrack density, defined in terms of the microcrack half-length (a) and the number of microcracks per unit area, *N*.[17]

Given the stiffness reduction for the angle-ply (±θ) layer as a function of the damage density, the effective stiffness of the $[90/(\pm\theta)]_s$ laminate can be calculated from simple laminate analysis. Figure 19 plots the reduction in effective modulus of the $[90/(\pm\theta)]_s$ laminate as a function of the damage parameter, ω. Results are computed for three cases, θ =10°, 15° and 20°, that are typical of helical plies in a filament wound tank.

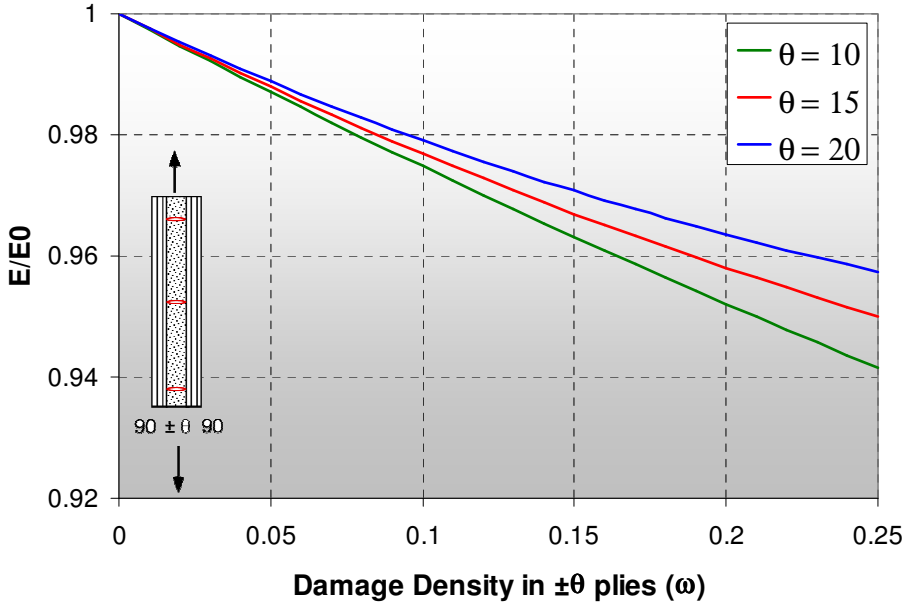

Figure 19: Reduction of the effective modulus of a $[90/(\pm\theta)]_s$ laminate with increase in microcrack density ω in the ±θ plies

Appendix D. Isostrain Dome Profile

Consider a filament-wound tank dome as shown in Figure 20. The dome profile is characterized by the radius, r and the dome height, z. The stress resultants in the composite shell when the tank dome is under internal pressure, p can be written as:[18]

$$N_\phi = \frac{pR_2}{2} = A_{11}\varepsilon_\phi + A_{12}\varepsilon_\theta$$
$$N_\theta = \frac{pR}{2}\left(2 - \frac{R_2}{R_1}\right) = A_{12}\varepsilon_\phi + A_{22}\varepsilon_\theta \qquad \text{(D1)}$$

where, N_ϕ, N_θ are the meridional and circumferential stress resultants, $\varepsilon_\phi, \varepsilon_\theta$ are the meridional and circumferential strains and R_1, R_2 are the principal radii of curvature of the dome as shown in Figure 20. The parameters A_{ij}, i=1,2 are the in-plane laminate stiffness resultants, which can be determined from composite laminate theory at each point in the dome and depend on the laminate architecture at that point.

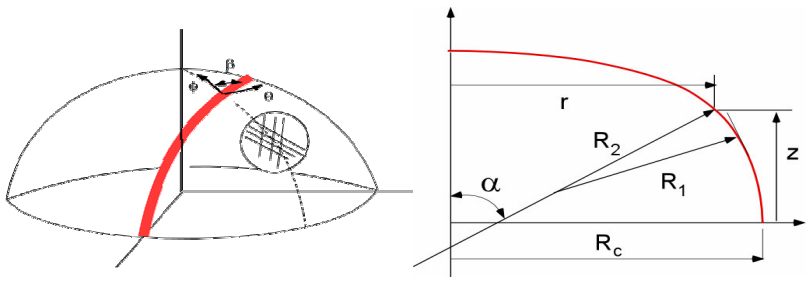

Figure 20: Geometry of filament wound dome profile.

The equations relating the shell strains $\varepsilon_\phi, \varepsilon_\theta$ to the strains $\varepsilon_1, \varepsilon_2$, along and across the fibers, and to the in plane shear strain ε_{12} are:

$$\begin{aligned} \varepsilon_1 &= \varepsilon_\phi \cos^2\beta + \varepsilon_\theta \sin^2\beta \\ \varepsilon_2 &= \varepsilon_\phi \sin^2\beta + \varepsilon_\theta \cos^2\beta \\ \varepsilon_{12} &= (\varepsilon_1 - \varepsilon_2)\sin 2\beta \end{aligned} \tag{D2}$$

where, β is the angle of the fiber orientation with respect to the meridional axis and changes continuously along the dome in a helical wind pattern (see Figure 20).

If the dome is designed such that the fibers are placed along the directions of the principal stresses in each layer, the shear stress and the shear strain in each layer can be assumed to be zero. Therefore,

$$\varepsilon_{12} = 0, \varepsilon_1 = \varepsilon_2 = \varepsilon_\phi = \varepsilon_\theta = \varepsilon \tag{D3}$$

A composite shell that can maintain the above relationship can be called an *isostrain* dome, such that the strain at each point on the dome, both along and across the fiber direction, is a constant, ε.

The constitutive equations for an orthotropic material are given as:

$$\begin{aligned} \sigma_1 &= \overline{E_1}(1+\nu_{21})\varepsilon \\ \sigma_2 &= \overline{E_2}(1+\nu_{12})\varepsilon \end{aligned} \tag{D4}$$

where,

$$\overline{E_i} = \frac{E_i}{1-\nu_{12}\nu_{21}}, i = 1,2$$

Solving eq. (D1) with eq. (D3) and substituting the result in eq. (D4), the principal stresses in the shell are obtained as:

$$\begin{aligned} \sigma_1 &= \frac{\overline{E_1}(1+\nu_{21})(N_\phi + N_\theta)}{h\left[\overline{E_1}(1+\nu_{21}) + \overline{E_2}(1+\nu_{12})\right]} \\ \sigma_2 &= \frac{\overline{E_2}(1+\nu_{12})(N_\phi + N_\theta)}{h\left[\overline{E_1}(1+\nu_{21}) + \overline{E_2}(1+\nu_{12})\right]} \end{aligned} \tag{D5}$$

It follows directly from eq. (D5) that the ratio of the stress in the fiber direction and that in the direction perpendicular to the fibers at any point on the isostrain dome is given by:

$$\frac{\sigma_2}{\sigma_1} = \frac{E_2(1+\nu_{12})}{E_1(1+\nu_{21})} = k \tag{D6}$$

The optimized profile of an isostrain dome can be determined from eqs. (D1), (D3) and radius of curvature of the shell, resulting in the following differential equation:

$$\frac{rz''}{z'\left[1+(z')^2\right]} = 2 - \frac{1-(1-k)\cos^2\beta}{k+(1-k)\cos^2\beta} \tag{D7}$$

The shape of the dome profile is determined by integrating equation (D7):

$$z(r) = \int_r^{R_c} \frac{1}{\sqrt{\left\{\frac{k+(1-k)\cos^2\beta}{k+(1-k)\cos^2\beta_0}\frac{R_c^2\cos\beta_0}{r^2\cos\beta}\right\}^2 - 1}} dr \tag{D8}$$

The variation of the fiber orientation angle, β is determined from:

$$\frac{r}{R_c} = \frac{\cos^k \beta_0 \left[1-(1-k)\cos^2 \beta_0\right]^{(1-k)/2}}{\cos^k \beta \left[1-(1-k)\cos^2 \beta\right]^{(1-k)/2}} \tag{D9}$$

In eqs. (D7) and (D8) $r=R_c$ and $\beta = \beta_0$ when z=0.

Acknowledgments

This material is based upon work supported by the United States Air Force under Contract No. HQ0006-04-C-7069, HQ0006-04-C-7070, FA9453-03-C-0211 and FA9453-03-C-0213. Any opinions, findings and conclusions or recommendations expressed in this material are those of the author(s) and do not necessarily reflect the views of the United States Air Force.

References

1. Peters, S.T., Humphrey, W.D. and Foral, R.F., *Filament Winding Composite Structure Fabrication*, 2nd ed., SAMPE publication,1987.
2. Robinson, M. J., "Composite Cryogenic Tank Development", 35th Structures, *Structural Dynamics, and Materials Conference and Adaptive Structures Forum*, 1994.
3. Mallick, K., Tupper, M. L., Arritt, B. J. and Paul C., "Thermo-micromechanics of Microcracking in a Composite Cryogenic Pressure Vessel", 44th AIAA/ASME/ASCE/AHS/ASC Structures, Structural Dynamics & Materials Conference, Norfolk, Virginia, 7-10 April, 2003.
4. Nairn, John A., "Matrix Microcracking in Composites," *Polymer Matrix Composites*, Elsevier Science, R. Talreja and J-A, Manson eds., Chapter 13, 2001.
5. Nairn, John A., "The Strain Energy Release Rate of Composite Microcracking: A Variational Approach", *Journal of Composite Materials*., Vol. 23, pp 1106-1129, 1989.
6. Mallick, K. et al., "Ultralight Linerless Composite Tanks for In-Space Applications," presented at the AIAA Space 2004 Conference, San Diego, Sept. 27-30, 2004.
7. Roth, A. *Vacuum Technology*, North Holland Publishing, New York, 1976.
8. Bechel, V. T. and Kim, R. Y., "Through Laminate Damage in Cryogenically Cycled Polymer Composites", 45th AIAA/ASME/ASCE/AHS/ASC Structures, Structural Dynamics & Materials Conference, Palm Springs, California, 19-22 April 2004.
9. Nairn, J. A. and Hu, S., "The Formation and Effect of Outer-Ply Microcracks in Cross-Ply Laminates: A Variational Approach", *Engineering Fracture Mechanics*, Vol. 41, 203-221, 1992
10. Roy, S. and Benjamin, M., "Modeling of Permeation and Damage in Graphite/Epoxy Laminates for Cryogenic Fuel Storage", *Composites Science and Technology*, Vol. 64, 2051-2065, 2004.
11. Noh., J., et al., "Numerical Modeling of Cryogen Leakage through Composite Laminates," AIAA paper 2004-1862, 45th AIAA/ASME/ASCE/AHS/ASC Structures, Structural Dynamics & Materials Conference, Palm Springs, California, 19 - 22 April 2004.
12. ABAQUS Analysis User's Manual, v. 6.5-1, 2004.
13. McCartney, L. N., "Predicting transverse crack formation in cross- ply laminates resulting from micro-cracking", *Composite Science and Technology*, Vol. 58, pp. 1069-81, 1998.
14. R. Joffe and J. Varna, "Analytical Modeling of Stiffness Reduction in Symmetric and Balanced Laminates due to Cracks in 90° Layers", Composites Science and Technology, 1999, Vol. 59, pp. 1641-1652.
15. R. Joffe and J. Varna, "Damage Evolution Modeling in Multidirectional Laminates and the Resulting Nonlinear Response", Proceedings of ICCM-12, 5-9 July, 1999, Paris, France.
16. Sumarac, D., Krajcinovic, D. and Mallick, K.,"Elastic Parameters of Brittle, Elastic Solids Containing Slits – Mean Field Theory," *International Journal of Damage Mechanics*, Vol. 1, pp. 320-346, 1992.
17. Budiansky, B. and Connell, R. J., "Elastic Moduli of a Cracked Solid," *International Journal of Solids and Structures*, Vol. 12, 81-97, 1976.
18. Bukanov, V. A. and Protasov, V. D., "Composite Pressure Vessels," Chapter 9, in *Handbook of Composites*, Vol. 2 - Structure and Design, Elsevier Science Publishers, 1989.